Jos Journal of Applied Animal Science & Environmental Stability 2026; 1(1):232-257

Jos Jornal of Applied Animal Science and Environmental Stability

Department of Animal Science. University of Jos.

IN SILICO AND TOXICOLOGICAL EVALUATION OF OREGANO (*Origanum vulgare*) PHYTOCHEMICALS AS INHIBITORS OF METHIONYL-tRNA SYNTHETASE OF *Brucella melitensis*

Oshibanjo, Olusegun Debola*[1], Ngurukwem, H. C.[1], Ugwu Ben Kingsley and Oyinlola, O. O[2]

[1]Department of Animal Science, Faculty of Agriculture, University of Jos, Jos, Plateau State, Nigeria

[2]Department of Animal Production Technology, Oyo State College of Agriculture and Technology, PMB 10, Igboora. Oyo State, Nigeria

*Corresponding author: oshibanjoo@unijos.edu.ng

Tel: +2348055438564

ABSTRACT

Brucellosis remains a neglected zoonosis of major veterinary and public health importance in Nigeria and across sub-Saharan Africa, and the long, relapse-prone antibiotic regimens currently in use have sustained interest in alternative antibacterial scaffolds. Methionyl-tRNA synthetase of *Brucella melitensis* (*Bm*MetRS) has been experimentally validated as a drug target for the disease. This study screened ten phenolic and flavonoid constituents of oregano (*Origanum vulgare*) against *Bm*MetRS and profiled their predicted pharmacokinetic and toxicological behaviour. Ligands were prepared with LigPrep and the crystal structure of *Bm*MetRS (PDB ID: 4PY2, 2.15 Å) with the Protein Preparation Wizard in the Schrödinger Suite 2023. Docking was carried out with Glide, drug-likeness and pharmacokinetics with SwissADME, and fifteen toxicity endpoints with ProTox. All ten phytochemicals docked into the *Bm*MetRS active site within a narrow affinity band of −6.35 to −6.59 kcal/mol, a range too small to rank the compounds reliably but sufficient to indicate that the flavonoid fraction of oregano engages the site as a class. Binding was anchored consistently at ASP 51, with MET 227, TYR 14 and TYR 228 recurring across ligands through hydrogen bonding and π–π stacking. Nine of the ten compounds showed high predicted gastrointestinal absorption, none violated Lipinski's rule of five, and bioavailability scores of 0.55–0.56 exceeded that of streptomycin (0.17). Predicted acute oral LD_{50} values

separated the compounds far more sharply than affinity did, ranging from 159 mg/kg (quercetin, class 3) to 5000 mg/kg (rosmarinic acid, class 5). Taking affinity, absorption and predicted safety together, kaempferol, apigenin, luteolin and rosmarinic acid emerged as the most balanced candidates. These are computational predictions and require *in vitro* confirmation, including assessment of selectivity against human methionyl-tRNA synthetase, before any therapeutic inference can be drawn.

Keywords: brucellosis; *Origanum vulgare*; methionyl-tRNA synthetase; molecular docking; ADMET prediction; flavonoids

1.0 INTRODUCTION

Zoonotic diseases are naturally transmissible infections shared between animals and humans, and they remain a persistent global public health burden. Agricultural expansion, urbanisation and environmental change have intensified human–animal contact in recent decades, sustaining the persistence and emergence of zoonotic infections worldwide. The burden falls disproportionately on developing regions where veterinary and public health surveillance systems are weakest (Rahman *et al.*, 2020; World Health Organization, 2022a).

Brucellosis is among the most widespread bacterial zoonoses and continues to impose substantial health and economic costs. It is caused by members of the genus *Brucella*, which infect cattle, goats, sheep and pigs and are transmitted to humans through direct contact with infected animals, consumption of unpasteurised dairy products, or inhalation of contaminated aerosols in occupational settings (Pappas *et al.*, 2005; World Health Organization, 2022a). The disease remains endemic across much of Africa, Asia and Latin America, where inadequate surveillance, limited vaccination coverage and weak food safety enforcement sustain transmission (Hull and Schumaker, 2020; McDermott *et al.*, 2021).

In Nigeria, brucellosis is endemic and remains largely uncontrolled. A national meta-analysis covering 2001–2021 estimated seroprevalence at 17.6% in humans and 13.3% in domestic animals, with the animal burden markedly higher in the north (15.8%) than in the south (8.7%), and reports drawn from 27 of the 36 states (Akinyemi *et al.*, 2022). A more recent meta-analysis restricted to Nigerian livestock placed pooled prevalence at 12.0% (95% CI: 10.0–14.0%) and attributed a substantial share of the variation between studies to differences in diagnostic method rather than to genuine epidemiological difference (Gaddafi *et al.*, 2026). Plateau State is itself affected. A serological survey of 270 cattle across four local government areas of northern Plateau, tested at the *Brucella* Research Laboratory of the National Veterinary Research Institute, Vom, returned an overall seroprevalence of 9.6%, rising to 37.3% in Bassa

Local Government Area and to 11.6% among cattle held under extensive pastoral management, against 3.1% under intensive management (Maurice *et al.,* 2013). Exposure in the region is therefore sustained by close herd contact, by the movement and trade of largely untested cattle, and by the consumption of unpasteurised milk and *nono*. Control is further constrained by the absence of a functioning national eradication programme and by the diagnostic overlap between brucellosis and malaria and typhoid, which dominate the differential diagnosis of febrile illness in the region.

Human brucellosis presents non-specifically, with intermittent fever, fatigue, arthralgia and general weakness that closely mimic other febrile illnesses, leading to frequent misdiagnosis and delayed treatment. Untreated or inadequately treated infection progresses to chronic multi-organ disease with long-term sequelae (Dean *et al.,* 2020; Zheng *et al.,* 2021a).

Treatment requires prolonged combination antibiotic therapy. The intracellular niche occupied by *Brucella* species shields the organism from immune clearance and limits antibiotic efficacy, while extended regimens, adverse drug effects and post-therapy relapse complicate case management further (Bagheri Nejad *et al.,* 2020; Ferri *et al.,* 2022). These constraints, compounded by the wider rise of antimicrobial resistance, have renewed interest in plant-derived antibacterial compounds, which offer structural diversity beyond that of established antibiotic scaffolds. Oregano (*Origanum vulgare*) is one such plant; its essential oil fraction, dominated by carvacrol and thymol, disrupts bacterial membranes, while its phenolic and flavonoid fraction has documented antibacterial and antioxidant activity (Sharifi-Rad *et al.,* 2021a).

Computational screening has become a standard first step in natural product drug discovery, allowing large compound sets to be evaluated against a defined molecular target before laboratory resources are committed (Lavecchia, 2021a; Sliwoski *et al.,* 2022). Its value depends on the quality of the target chosen. Methionyl-tRNA synthetase of *B. melitensis* (*Bm*MetRS) is a strong candidate: it is essential for protein synthesis and bacterial survival, its inhibition arrests growth of *B. melitensis* strain 16M, and inhibitor-bound crystal structures are available (Ojo *et al.,* 2016).

Despite this, the phenolic constituents of *O. vulgare* have not been evaluated against *Bm*MetRS, and published oregano docking studies rarely couple affinity estimates with predicted toxicity, so compounds that bind well but carry unfavourable safety profiles are not filtered out before experimental work begins. The present study therefore set out to dock ten phenolic and flavonoid constituents of *O. vulgare* against *Bm*MetRS, characterise the residue-level interactions underlying binding, predict the pharmacokinetic

and drug-likeness properties of the compounds, profile them across fifteen toxicity endpoints, and integrate the three data streams to identify candidates warranting laboratory validation.

2.0 MATERIALS AND METHODS

2.1 Computational facility and software

All computational work was carried out in the Department of Animal Science, Faculty of Agriculture, University of Jos, Plateau State, Nigeria, using the Schrödinger Suite 2023 (Schrödinger LLC, New York, USA), together with the publicly accessible SwissADME and ProTox web servers.

2.2 Selection and preparation of ligands

Ten phenolic and flavonoid constituents of *O. vulgare* — scutellarein, quercetin, eriodictyol, kaempferol, naringenin, apigenin, luteolin, taxifolin (dihydroquercetin), hesperetin and rosmarinic acid — were obtained from PubChem database. Streptomycin (PubChem CID 19649) was used as the reference antibacterial.

Canonical SMILES and structure data files were retrieved from the PubChem database and imported into the Schrödinger Suite 2023 workspace. Ligands were prepared with LigPrep, generating low-energy three-dimensional conformers with correct chiralities. Ionisation states were generated at physiological pH 7.2 ± 0.2 ionisation module, typically Epik, stereoisomers were enumerated by retaining specified chiralities and varying the remainder, and the resulting structures were energy-minimised using the OPLS4 force field prior to docking.

2.3 Preparation of the receptor

The crystal structure of methionyl-tRNA synthetase from *B. melitensis* in complex with a thiophenyl-urea inhibitor (PDB ID: 4PY2; X-ray diffraction; resolution 2.15 Å; R-free 0.211; R-work 0.178) was retrieved from the Protein Data Bank and imported into the Schrödinger Suite 2023 workspace. The structure was processed with the Protein Preparation Wizard: non-standard residues, ions, crystallographic water molecules and bound ligands were removed, hydrogen atoms were added, bond orders were assigned, and the structure was subjected to restrained minimisation to an RMSD.

2.4 Receptor grid generation

A receptor grid defining the size and position of the active site was generated with the Receptor Grid Generation tool in Schrödinger Maestro 13.5, centred on the co-crystallised inhibitor [AUTHOR TO

CONFIRM: HET code 43E in 4PY2; the manuscript refers to this ligand as "GK"]. The grid was centred at X = 28.64, Y = 6.67, Z = 11.73.

2.5 Molecular docking and protocol validation

Prepared ligands were docked into the receptor grid using Glide ligand docking. Docking scores were extracted from the Maestro project table. Compounds were considered valid hits only where the ligand occupied the same site as the reference. Two- and three-dimensional ligand interaction diagrams were generated within the suite to identify the bond types and interacting residues within the binding site.

2.6 Prediction of pharmacokinetic and drug-likeness properties

Absorption, distribution, metabolism and excretion properties were predicted using the SwissADME server (Daina *et al.*, 2017). Lipophilicity was expressed as the consensus log P, the arithmetic mean of values predicted by the XLOGP3, WLOGP, MLOGP, iLOGP and SILICOS-IT models. Water solubility was predicted as the logarithm of molar solubility (log S) using the ESOL, Ali and SILICOS-IT models. Drug-likeness was assessed against the Lipinski, Ghose, Veber, Egan and Muegge rule-based filters. Pharmacokinetic descriptors comprised gastrointestinal absorption, blood–brain barrier permeation, P-glycoprotein substrate status and cytochrome P450 isoform inhibition. Medicinal chemistry friendliness was assessed through PAINS and Brenk structural alerts, lead-likeness violations and synthetic accessibility scores.

2.7 Toxicity prediction

Acute oral toxicity and organ- and mechanism-specific toxicity endpoints were predicted using the ProTox server, ProTox-II or ProTox-3.0 (Banerjee *et al.*, 2018). Predicted median lethal dose (LD_{50}, mg/kg) and the corresponding Globally Harmonised System toxicity class were recorded. Fifteen endpoints were evaluated: hepatotoxicity, neurotoxicity, nephrotoxicity, respiratory toxicity, cardiotoxicity, carcinogenicity, immunotoxicity, mutagenicity, cytotoxicity, blood–brain barrier penetration, ecotoxicity, clinical toxicity, nutritional toxicity and heat shock factor response element (HSE) activation. Each endpoint was returned as active or inactive.

2.8 Data handling

Docking scores are reported in kcal/mol, with more negative values denoting more favourable predicted binding. Because Glide scoring functions are not reproducible to a resolution finer than approximately 1 kcal/mol, compounds separated by less than this margin are treated in this study as an equivalent affinity

band rather than rank-ordered, and lead selection is driven by the integration of affinity with pharmacokinetic and toxicity predictions.

3.0 RESULTS

3.1 Docking scores, acute toxicity and toxicity class

Docking scores, predicted acute oral LD_{50} values and toxicity classes for streptomycin and the ten phytochemicals are presented in Table 1. All ten phytochemicals returned negative docking scores confined to a 0.24 kcal/mol band, from −6.59 kcal/mol (scutellarein) to −6.35 kcal/mol (rosmarinic acid). Streptomycin returned a value of 6.21.

Predicted acute toxicity varied over a far wider range than affinity. Rosmarinic acid returned the highest LD_{50} (5000 mg/kg, class 5), followed by scutellarein, kaempferol and luteolin (3919 mg/kg, class 5) and apigenin (2500 mg/kg, class 5). Eriodictyol, naringenin, taxifolin and hesperetin were class 4 (2000 mg/kg). Quercetin returned the lowest LD_{50} of all compounds tested (159 mg/kg, class 3), below that of streptomycin (500 mg/kg, class 3).

Table 1: Docking scores, predicted acute oral LD_{50} and toxicity class of the reference drug and oregano phytochemicals

Compound	PubChem CID	LD_{50} (mg/kg)	Toxicity class	Docking score (kcal/mol)
Streptomycin (reference)	19649	500	3	-6.21
Scutellarein	5281697	3919	5	−6.59
Quercetin	5280343	159	3	−6.58
Eriodictyol	440735	2000	4	−6.57
Kaempferol	5280863	3919	5	−6.56
Naringenin	439246	2000	4	−6.55
Apigenin	5280443	2500	5	−6.55
Luteolin	5280445	3919	5	−6.54
Taxifolin (dihydroquercetin)	439533	2000	4	−6.51
Hesperetin	72281	2000	4	−6.43

Compound	PubChem CID	LD_{50} (mg/kg)	Toxicity class	Docking score (kcal/mol)
Rosmarinic acid	5281792	5000	5	−6.35

3.2 Ligand–receptor interactions

Interacting residues and bond types are summarised in Table 2. Streptomycin formed hydrogen bonds with ASP 51, ASP 264, GLU 26 and ILE 12. The phytochemicals engaged the site through a combination of hydrogen bonding and π–π stacking. ASP 51 was involved in the binding of every compound examined. Scutellarein, quercetin, eriodictyol, naringenin, taxifolin and hesperetin each interacted with ASP 51, MET 227 and TYR 14; kaempferol, apigenin and luteolin additionally engaged TYR 228, giving four contact residues. Rosmarinic acid interacted with ASP 51, ASP 264, MET 227 and TYR 228, sharing ASP 264 with streptomycin. All ligands presented negatively charged and hydrophobic contact character.

Table 2: Interacting residues, bond types and contact character of the reference drug and oregano phytochemicals at the BmMetRS binding site

Ligand	Interacting amino acid residues	Bond types	Contact character
Streptomycin	ASP 51, ASP 264, GLU 26, ILE 12	Hydrogen bond	Charged (negative), hydrophobic
Scutellarein	ASP 51, MET 227, TYR 14	Hydrogen bond, π–π stacking	Charged (negative), hydrophobic
Quercetin	ASP 51, MET 227, TYR 14	Hydrogen bond, π–π stacking	Charged (negative), hydrophobic
Eriodictyol	ASP 51, MET 227, TYR 14	Hydrogen bond, π–π stacking	Charged (negative), hydrophobic
Kaempferol	ASP 51, MET 227, TYR 14, TYR 228	Hydrogen bond, π–π stacking	Charged (negative), hydrophobic
Naringenin	ASP 51, MET 227, TYR 14	Hydrogen bond, π–π stacking	Charged (negative), hydrophobic
Apigenin	ASP 51, MET 227, TYR 14, TYR 228	Hydrogen bond, π–π stacking	Charged (negative), hydrophobic
Luteolin	ASP 51, MET 227, TYR 14,	Hydrogen bond, π–	Charged (negative),

Ligand	Interacting amino acid residues	Bond types	Contact character
	TYR 228	π stacking	hydrophobic
Taxifolin	ASP 51, MET 227, TYR 14	Hydrogen bond, π–π stacking	Charged (negative), hydrophobic
Hesperetin	ASP 51, MET 227, TYR 14	Hydrogen bond, π–π stacking	Charged (negative), hydrophobic
Rosmarinic acid	ASP 51, ASP 264, MET 227, TYR 228	Hydrogen bond, π–π stacking	Charged (negative), hydrophobic

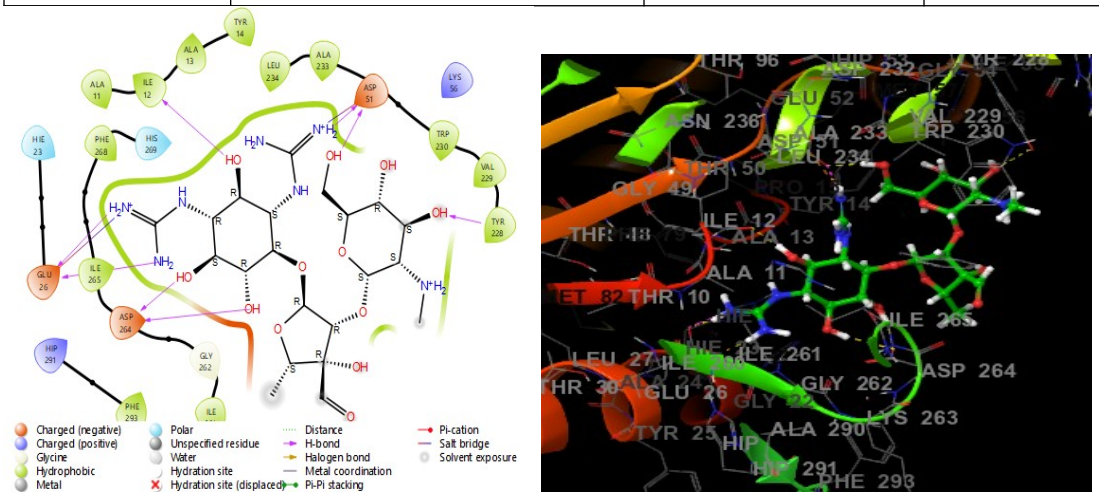


Figure 1: 2D and 3D of crystal structure of methionyl-tRNA synthetase MetRS from Brucella melitensis (4PY2) with Streptomycin

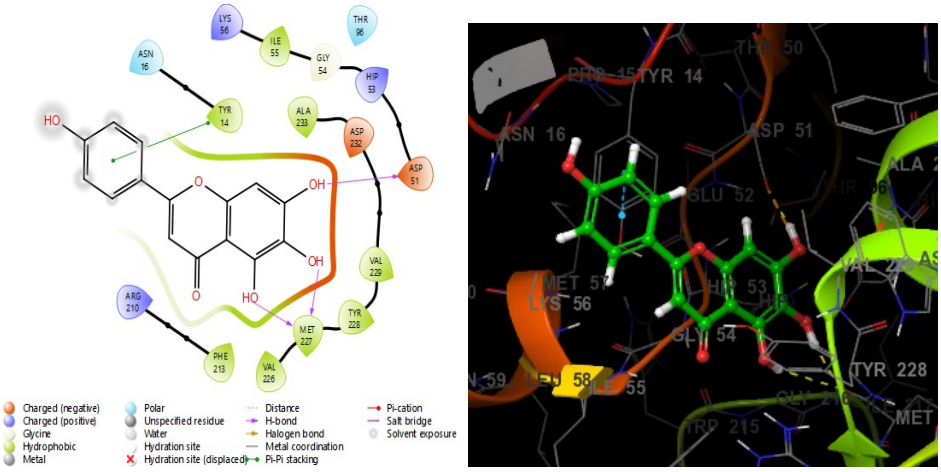


Figure 2: 2D and 3D of crystal structure of methionyl-tRNA synthetase MetRS from Brucella melitensis (4PY2) with Scutellarein

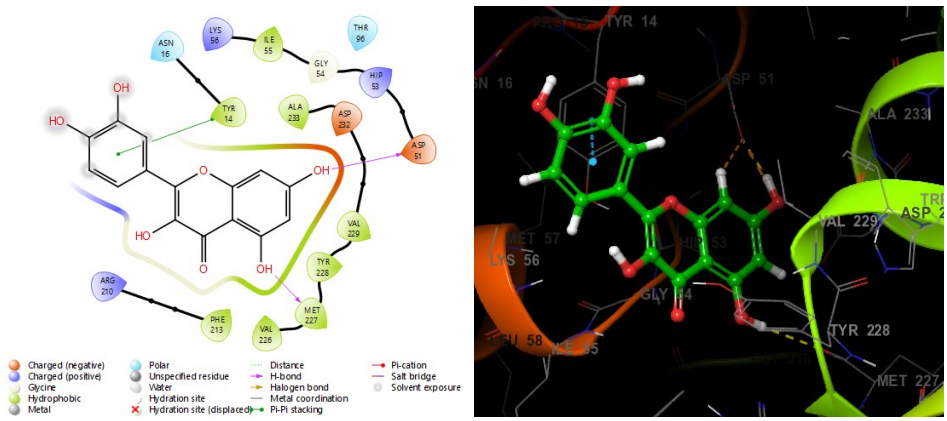


Figure 3: 2D and 3D of crystal structure of methionyl-tRNA synthetase MetRS from Brucella melitensis (4PY2) with **Quercetin**

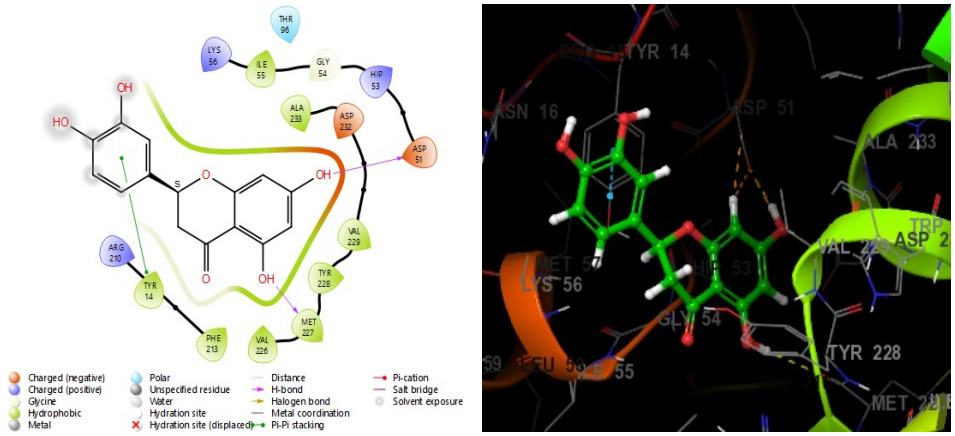


Figure 4: 2D and 3D of crystal structure of methionyl-tRNA synthetase MetRS from Brucella melitensis (4PY2) with Eriodictyol

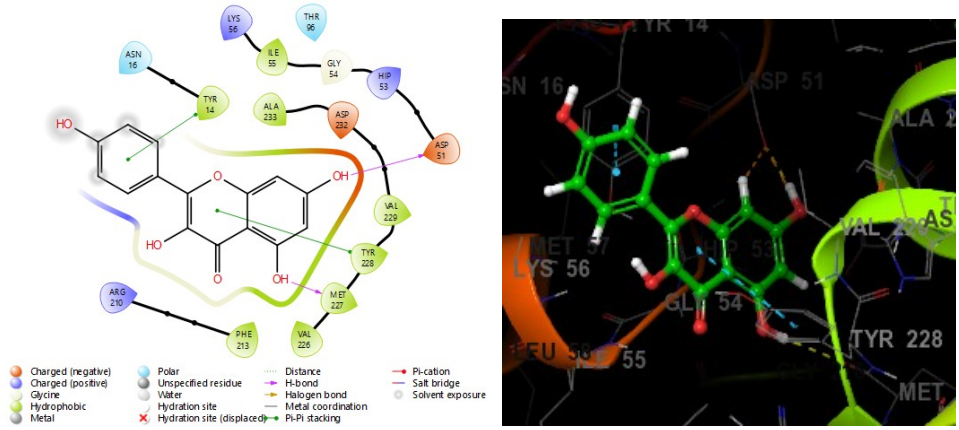


Figure 5: 2D and 3D of crystal structure of methionyl-tRNA synthetase MetRS from Brucella melitensis (4PY2) with Kaempferol

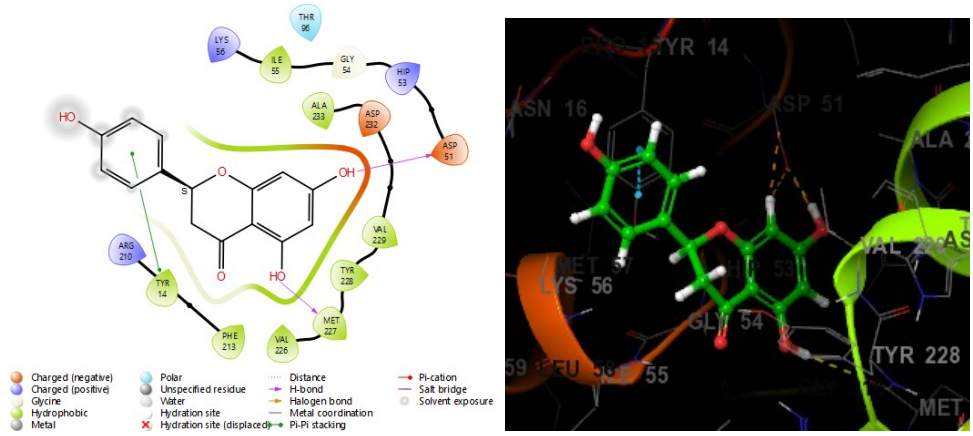


Figure 6: 2D and 3D of crystal structure of methionyl-tRNA synthetase MetRS from Brucella melitensis (4PY2) with Naringenin

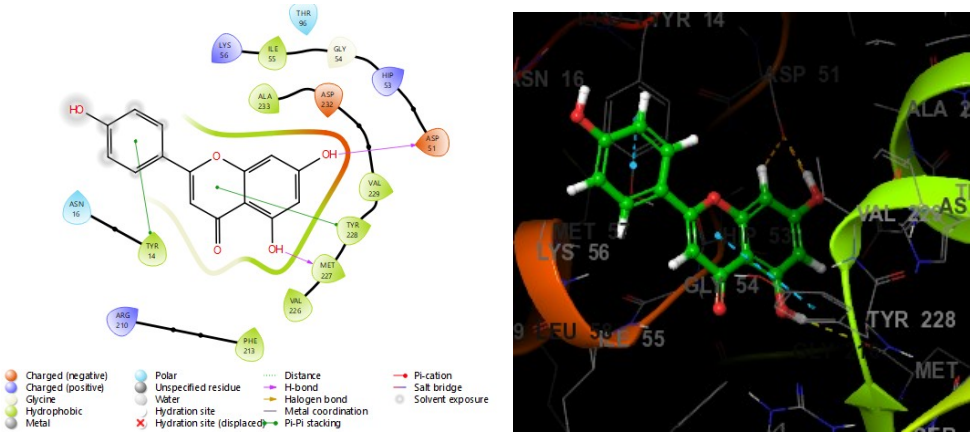


Figure 7: 2D and 3D of crystal structure of methionyl-tRNA synthetase MetRS from Brucella melitensis (4PY2) with Apigenin

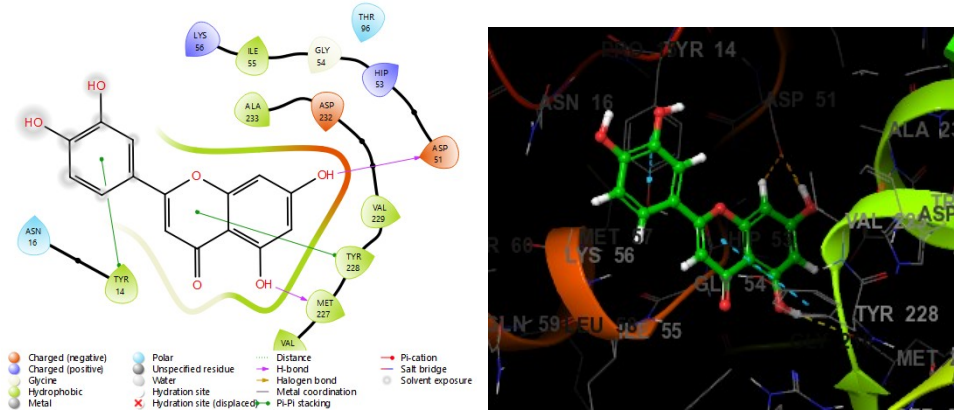


Figure 8: 2D and 3D of crystal structure of methionyl-tRNA synthetase MetRS from Brucella melitensis (4PY2) with Luteolin

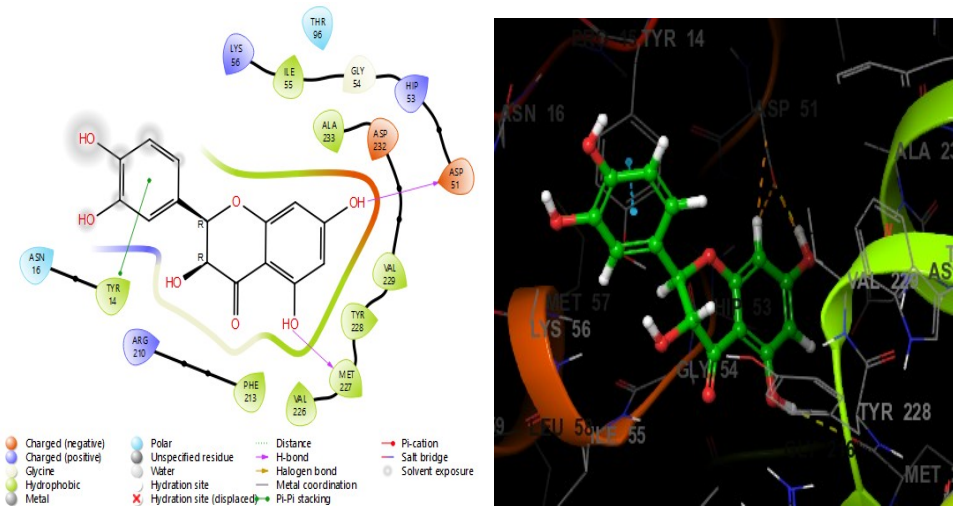


Figure 9: 2D and 3D of crystal structure of methionyl-tRNA synthetase MetRS from Brucella melitensis (4PY2) with Taxifolin (Dihydroquercetin)

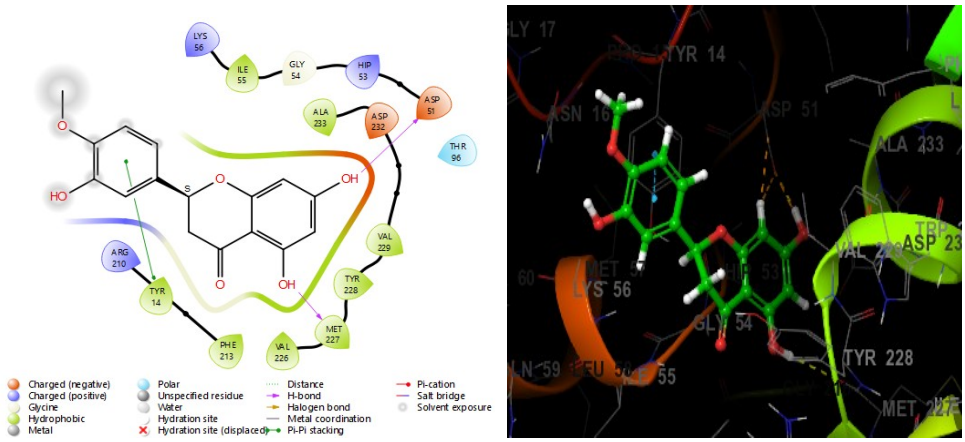


Figure 10: 2D and 3D of crystal structure of methionyl-tRNA synthetase MetRS from Brucella melitensis (4PY2) with Hesperetin

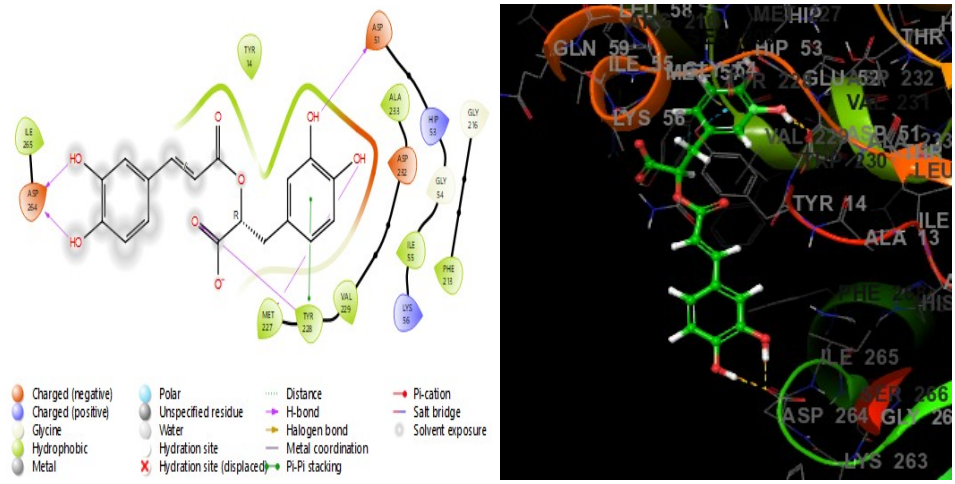


Figure 11: 2D and 3D of crystal structure of methionyl-tRNA synthetase MetRS from Brucella melitensis (4PY2) with Rosmarinic acid

3.3 Predicted pharmacokinetic and drug-likeness properties

Predicted ADME and drug-likeness parameters are presented in Table 3. Molecular weights ranged from 270.24 g/mol (apigenin) to 581.57 g/mol (streptomycin). All phytochemicals were predicted soluble or highly soluble across the three solubility models, with hesperetin and rosmarinic acid rated moderately soluble by the Ali model. Gastrointestinal absorption was predicted high for nine of the ten phytochemicals; rosmarinic acid and streptomycin were predicted low. None of the compounds, including streptomycin, was predicted to permeate the blood–brain barrier.

No phytochemical violated the Lipinski, Ghose or Muegge filters; rosmarinic acid returned single violations of the Veber, Egan and lead-likeness criteria. Streptomycin returned three Lipinski, four Ghose, one Veber, one Egan and four Muegge violations. Bioavailability scores were 0.55 for all phytochemicals except rosmarinic acid (0.56), against 0.17 for streptomycin. PAINS alerts were returned for scutellarein, quercetin, eriodictyol, luteolin, taxifolin and rosmarinic acid. Synthetic accessibility scores for the phytochemicals ranged from 2.96 to 3.51, against 6.92 for streptomycin.

3.4 Predicted toxicity profiles

Predicted activity across the fifteen toxicity endpoints is presented in Table 4. No compound, including streptomycin, was predicted hepatotoxic, and none was predicted to activate the heat shock factor response element. All eleven compounds were predicted nephrotoxic. Respiratory toxicity was predicted active for all compounds except rosmarinic acid. Streptomycin was the only compound predicted neurotoxic, and hesperetin the only compound predicted cardiotoxic. Naringenin was the only compound predicted cytotoxic.

Carcinogenicity was predicted for scutellarein, quercetin, eriodictyol, luteolin and taxifolin, and mutagenicity for streptomycin, scutellarein, quercetin, luteolin and taxifolin. Immunotoxicity was predicted for hesperetin and rosmarinic acid. Blood–brain barrier activity was returned for all compounds except streptomycin, apigenin and hesperetin. Ecotoxicity was predicted for naringenin and apigenin, clinical toxicity for streptomycin, eriodictyol, naringenin, hesperetin and rosmarinic acid, and nutritional toxicity for all compounds except streptomycin, apigenin and rosmarinic acid.

Table 3: Predicted absorption, distribution, metabolism, excretion and drug-likeness properties of the reference drug and oregano phytochemicals

Parameter	Streptomycin	Scutellarein	Quercetin	Eriodictyol	Kaempferol	Naringenin	Apigenin	Luteolin	Taxifolin	Hesperetin	Rosmarinic acid
Molecular weight (g/mol)	581.57	286.24	302.24	288.25	286.24	272.25	270.24	286.24	304.25	302.28	360.31
ESOL class	Highly soluble	Soluble	Soluble	Soluble	Soluble	Soluble	Soluble	Soluble	Soluble	Soluble	Soluble
Ali class	Highly soluble	Soluble	Soluble	Soluble	Soluble	Soluble	Soluble	Soluble	Soluble	Moderately soluble	Moderately soluble
SILICOS-IT class	Soluble	Soluble	Soluble	Soluble	Soluble	Soluble	Soluble	Soluble	Soluble	Soluble	Soluble
GI absorption	Low	High	High	High	High	High	High	High	High	High	Low
BBB permeant	No	No	No	No	No	No	No	No	No	No	No
Lipinski violations	3	0	0	0	0	0	0	0	0	0	0
Ghose violations	4	0	0	0	0	0	0	0	0	0	0
Veber violations	1	0	0	0	0	0	0	0	0	0	1
Egan violations	1	0	0	0	0	0	0	0	0	0	1
Muegge violations	4	0	0	0	0	0	0	0	0	0	0
Bioavailability score	0.17	0.55	0.55	0.55	0.55	0.55	0.55	0.55	0.55	0.55	0.56

Parameter	Streptomycin	Scutellarein	Quercetin	Eriodictyol	Kaempferol	Naringenin	Apigenin	Luteolin	Taxifolin	Hesperetin	Rosmarinic acid
PAINS alerts	0	1	1	1	0	0	0	1	1	0	1
Brenk alerts	3	1	1	1	0	0	0	1	1	0	2
Lead-likeness violations	2	0	0	0	0	0	0	0	0	0	1
Synthetic accessibility	6.92	3.04	3.23	3.11	3.14	3.01	2.96	3.02	3.51	3.22	3.38

GI = gastrointestinal; BBB = blood–brain barrier; PAINS = pan-assay interference compounds. Taxifolin = dihydroquercetin.

Table 4: Predicted toxicity endpoints of the reference drug and oregano phytochemicals

Endpoint	Streptomycin	Scutellarein	Quercetin	Eriodictyol	Kaempferol	Naringenin	Apigenin	Luteolin	Taxifolin	Hesperetin	Rosmarinic acid
Hepatotoxicity	Inactive	Inactive	Inactive	Inactive	Inactive	Inactive	Inactive	Inactive	Inactive	Inactive	Inactive
Neurotoxicity	Active	Inactive	Inactive	Inactive	Inactive	Inactive	Inactive	Inactive	Inactive	Inactive	Inactive
Nephrotoxicity	Active	Active	Active	Active	Active	Active	Active	Active	Active	Active	Active
Respiratory toxicity	Active	Active	Active	Active	Active	Active	Active	Active	Active	Active	Inactive
Cardiotoxicity	Inactive	Inactive	Inactive	Inactive	Inactive	Inactive	Inactive	Inactive	Inactive	Active	Inactive
Carcinogenicity	Inactive	Active	Active	Active	Inactive	Inactive	Inactive	Active	Active	Inactive	Inactive
Immunotoxicity	Inactive	Inactive	Inactive	Inactive	Inactive	Inactive	Inactive	Inactive	Inactive	Active	Active

Endpoint	Streptomycin	Scutellarein	Quercetin	Eriodictyol	Kaempferol	Naringenin	Apigenin	Luteolin	Taxifolin	Hesperetin	Rosmarinic acid
Mutagenicity	Active	Active	Active	Inactive	Inactive	Inactive	Inactive	Active	Active	Inactive	Inactive
Cytotoxicity	Inactive	Inactive	Inactive	Inactive	Inactive	Active	Inactive	Inactive	Inactive	Inactive	Inactive
BBB barrier	Inactive	Active	Active	Active	Active	Active	Inactive	Active	Active	Inactive	Active
Ecotoxicity	Inactive	Inactive	Inactive	Inactive	Inactive	Active	Active	Inactive	Inactive	Inactive	Inactive
Clinical toxicity	Active	Inactive	Inactive	Active	Inactive	Active	Inactive	Inactive	Inactive	Active	Active
Nutritional toxicity	Inactive	Active	Active	Active	Active	Active	Inactive	Active	Active	Active	Inactive
HSE activation	Inactive	Inactive	Inactive	Inactive	Inactive	Inactive	Inactive	Inactive	Inactive	Inactive	Inactive

BBB = blood–brain barrier; HSE = heat shock factor response element. Taxifolin = dihydroquercetin.

4.0 DISCUSSION

4.1 Binding affinity of oregano phytochemicals for BmMetRS

All ten phenolic and flavonoid constituents of *O. vulgare* docked favourably into the *Bm*MetRS active site, occupying the same pocket as the co-crystallised inhibitor. In docking analysis, more negative scores denote more stable predicted ligand–protein association and a higher likelihood of inhibitory activity (Lavecchia, 2021a). The finding of greatest substance here is not which compound scored highest but how little the compounds differed: the entire set spanned 0.24 kcal/mol. Glide scoring functions are empirical approximations, and differences of this magnitude fall well within the error of the method. The ten compounds are therefore best interpreted as an equivalent affinity band rather than a ranked series, and the ordering reported in Table 1 should not be read as a ranking of potency.

Interpreted this way, the result is informative in a different and arguably more useful way. That ten structurally related phenolics all engage the same site at comparable predicted affinity suggests that the *Bm*MetRS methionine-binding pocket accommodates the flavonoid scaffold as a class. This is consistent with the established structure–activity relationship of hydroxyl-rich flavonoids in antimicrobial discovery, in which multiple hydroxyl groups support hydrogen bonding while the fused aromatic ring system contributes hydrophobic and π-interactions (Atanasov *et al.*, 2021; Sharifi-Rad *et al.*, 2021a), and it supports the ethnomedicinal use of oregano as an antimicrobial plant on the basis of its combined phenolic content rather than any single constituent.

The findings align in a general way with Zhao *et al.* (2023), who identified quercetin, kaempferol and luteolin as high-affinity flavonoid binders in a network pharmacology study of adjuvant brucellosis treatment and showed experimentally that quercetin reduced intracellular *B. abortus* survival in THP-1 macrophages. The same three compounds fall within the present affinity band. Direct comparison of scores between the two studies is not appropriate, since Zhao *et al.* (2023) targeted host inflammatory proteins whereas the present study targeted a bacterial enzyme, and active-site geometry differs accordingly.

4.2 Residue-level interactions

Interaction type and residue engagement determine binding stability beyond what a single score conveys. Hydrogen bonding confers specificity, while hydrophobic and π–π stacking interactions contribute to the stability of the complex (Donadio *et al.*, 2021). ASP 51 participated in the binding of every ligand tested, including the reference drug, identifying it as the principal anchoring residue of the pocket. MET 227, TYR 14 and TYR 228 recurred across the flavonoids, indicating a shared binding mode within this compound class and reinforcing the interpretation advanced in section 4.1.

This pattern is consistent with Donadio *et al.* (2021), who attributed flavonoid antibacterial activity to combined hydrogen bonding and hydrophobic or aromatic contacts, with hydroxyl-rich flavonoids such as quercetin, luteolin, apigenin and kaempferol showing the strongest engagement. Hamzah *et al.* (2026) reported a comparable interaction signature for quercetin and kaempferol against a *Klebsiella pneumoniae* target — a different protein, but the same combination of contact types, which supports the view that flavonoids engage bacterial proteins through a conserved repertoire of interactions.

Kaempferol, apigenin and luteolin each engaged four residues, including TYR 228, one more than the remaining flavonoids. A greater number of contacts is generally associated with greater predicted complex stability (Ayodele and Sabiu, 2026), although in the absence of molecular dynamics simulation this remains an inference rather than a demonstration. Rosmarinic acid, structurally distinct from the flavonoids as a caffeic acid ester, shared ASP 264 with streptomycin while forming additional aromatic contacts unavailable to the aminoglycoside, consistent with the multi-target character commonly reported for plant polyphenols (Sharifi-Rad *et al.*, 2021a).

Residue identity is specific to the receptor, its active-site geometry and the docking protocol used, so comparisons of exact residues across studies targeting different proteins are of limited value. Comparison of interaction types is more meaningful, and on that basis the present results are in agreement with the flavonoid docking literature.

4.3 Predicted pharmacokinetic behaviour

Favourable binding is of no therapeutic value without acceptable pharmacokinetics, which is why computational ADME prediction is now a routine early filter in drug discovery (Daina *et al.*, 2017;

Atanasov *et al.*, 2021). Nine of the ten phytochemicals were predicted to have high gastrointestinal absorption, while streptomycin was predicted low — consistent with the poor oral bioavailability of aminoglycosides and their clinical administration by intramuscular injection (World Health Organization, 2023). Rosmarinic acid was the single phytochemical predicted to have low absorption, reflecting its higher polar surface area and its Veber and Egan violations; any development of this compound would require attention to formulation.

None of the phytochemicals violated the Lipinski, Ghose or Muegge filters, whereas streptomycin violated several, reflecting its size and high polarity against the more drug-like molecular weight, lipophilicity and hydrogen-bonding profile of the flavonoids (Lipinski *et al.*, 2001; Daina *et al.*, 2017). Bioavailability scores of 0.55–0.56 against 0.17 for streptomycin, and synthetic accessibility scores of 2.96–3.51 against 6.92, point to compounds that are both more orally tractable and considerably easier to obtain or synthesise than the reference drug — a consideration of real practical weight for resource-constrained settings where brucellosis is endemic.

No compound was predicted to cross the blood–brain barrier in the SwissADME model. For a predominantly peripheral infection this is not a liability, and reduced central nervous system exposure lowers the risk of neurological adverse effects. PAINS and Brenk alerts returned for six of the compounds should be read as flags for experimental caution, particularly in assay design, rather than as evidence of inactivity or toxicity (Baell and Holloway, 2010); flavonoids are frequent PAINS-flagged scaffolds by virtue of their catechol and phenolic substructures.

4.4 Predicted toxicity

Toxicity screening is applied alongside docking and ADME because attrition late in development is frequently driven by toxicity rather than by lack of activity (Atanasov *et al.*, 2021). None of the compounds was predicted hepatotoxic, a favourable finding given the central role of the liver in xenobiotic metabolism and drug attrition (Guengerich, 2022) and consistent with reports of generally low hepatotoxicity among plant flavonoids (Sharifi-Rad *et al.*, 2021a).

All eleven compounds, including streptomycin, were predicted nephrotoxic. For streptomycin this is consistent with well-characterised aminoglycoside-mediated renal tubular injury through oxidative stress (Lopez-Novoa *et al.*, 2011). For the phytochemicals, a uniform positive prediction across an entire structural class more plausibly reflects structural pattern-matching within the

model's training set than a genuine shared liability, and renal safety should be treated as an open question requiring experimental resolution rather than as an established finding. Streptomycin alone was predicted neurotoxic, consistent with its documented ototoxicity and neurotoxicity (World Health Organization, 2023).

Carcinogenicity and mutagenicity predictions were mixed and should be interpreted conservatively. Computational toxicity models are deliberately calibrated toward sensitivity and carry a correspondingly high false-positive rate (Banerjee *et al.*, 2018). Quercetin illustrates the difficulty: it was flagged for both endpoints and returned the lowest LD_{50} of any compound tested, yet the experimental literature also documents antioxidant and chemoprotective activity that varies with dose and cellular context (D'Andrea, 2015). Among the compounds tested, kaempferol and apigenin returned the smallest number of active endpoints, with kaempferol flagged only for nephrotoxicity, respiratory toxicity, blood–brain barrier penetration and nutritional toxicity, and apigenin only for nephrotoxicity, respiratory toxicity, ecotoxicity and nutritional toxicity. Rosmarinic acid was the only compound inactive for respiratory toxicity, and was inactive for hepatotoxicity, neurotoxicity, cardiotoxicity, carcinogenicity and mutagenicity, although it was flagged for immunotoxicity, nephrotoxicity and clinical toxicity; its LD_{50} of 5000 mg/kg is consistent with the favourable safety record reported for this compound (Petersen and Simmonds, 2023).

One apparent inconsistency warrants comment. Several compounds were returned as blood–brain barrier active by the toxicity model but non-permeant by SwissADME. This is not a contradiction so much as a reflection of two platforms using different algorithms, descriptors and training data. Experimental determination of central nervous system exposure would be required to resolve it (Daina *et al.*, 2017).

4.5 Integrated selection of lead candidates

Because binding affinity did not discriminate among the compounds, lead selection in this study rests on the pharmacokinetic and toxicity data, where the differences are substantial. On that basis, kaempferol, apigenin and luteolin combine high predicted gastrointestinal absorption, full compliance with all five drug-likeness filters, bioavailability scores of 0.55, favourable synthetic accessibility, class 5 acute toxicity and comparatively few active toxicity endpoints. Kaempferol

and apigenin are the strongest of the three, both being free of carcinogenicity and mutagenicity flags; luteolin returned both. Rosmarinic acid presents a different profile — the highest LD_{50} of the set and the cleanest organ-toxicity record, offset by low predicted gastrointestinal absorption that would constrain oral administration.

Quercetin illustrates the value of coupling affinity with safety prediction. Its docking score was indistinguishable from those of the leads, but its predicted LD_{50} of 159 mg/kg is the lowest of any compound examined and places it below streptomycin in the same toxicity class. Had affinity been the sole criterion, quercetin would have advanced to laboratory testing; the integrated approach identifies it instead as a compound requiring careful dose-ranging before any such commitment.

4.6 Limitations of the study

Several constraints bound the interpretation of these results. Docking scores are empirical estimates of binding free energy and are not reliable to the resolution at which the present compounds differ; no molecular dynamics simulation or MM-GBSA rescoring was performed to test the stability of the predicted poses over time. The receptor was treated as rigid, so induced-fit effects were not captured. ADME and toxicity outputs are statistical predictions derived from training sets whose chemical coverage of plant phenolics is uneven, and the uniform nephrotoxicity prediction across all eleven compounds is a plausible instance of this limitation.

Most importantly, selectivity was not assessed. Methionyl-tRNA synthetase is essential in humans as well as in bacteria, and the therapeutic case for *Bm*MetRS rests on the structural divergence between the bacterial enzyme and its mammalian orthologue (Ojo *et al.*, 2016). A compound that inhibits both offers no therapeutic window. Parallel docking against human cytoplasmic methionyl-tRNA synthetase is a necessary next step. Finally, no experimental work was undertaken; none of the predictions reported here has been confirmed against *Brucella* cultures, and the study should be read as a prioritisation exercise rather than as evidence of antibacterial activity.

5.0 CONCLUSION

Ten phenolic and flavonoid constituents of *Origanum vulgare* were predicted to bind the methionyl-tRNA synthetase of *Brucella melitensis* within a narrow and essentially equivalent

affinity band, anchored consistently at ASP 51 and stabilised by hydrogen bonding and π–π stacking involving MET 227, TYR 14 and TYR 228. The uniformity of this engagement suggests that the enzyme's active site accommodates the flavonoid scaffold as a structural class rather than favouring any single constituent. Differentiation among the compounds came instead from their predicted pharmacokinetic and toxicological profiles, on which kaempferol and apigenin offered the most favourable overall balance, followed by luteolin, while rosmarinic acid combined the cleanest predicted safety record with limited oral absorption. These findings are computational predictions and establish no antibacterial activity; they identify a defined set of compounds worth committing laboratory resources to.

6.0 RECOMMENDATIONS

1. Kaempferol, apigenin, luteolin and rosmarinic acid should be evaluated *in vitro* against *B. melitensis* and *B. abortus* isolates, with determination of minimum inhibitory and minimum bactericidal concentrations.
2. Inhibition of recombinant BmMetRS should be confirmed directly using an aminoacylation assay, to establish that any observed growth inhibition proceeds through the proposed mechanism.
3. Selectivity should be assessed against human cytoplasmic methionyl-tRNA synthetase, computationally in the first instance and enzymatically thereafter.
4. Molecular dynamics simulation and MM-GBSA rescoring should be applied to the lead complexes to test pose stability and refine binding energy estimates.
5. Predicted nephrotoxicity should be examined experimentally, given that it was returned for every compound screened.
6. Combination activity with doxycycline or streptomycin should be explored, since adjuvant use is a more realistic near-term application of plant phenolics than monotherapy.

REFERENCES

Akinyemi, K. O., Fakorede, C. O., Amisu, K. O., & Wareth, G. (2022). Human and animal brucellosis in Nigeria: A systematic review and meta-analysis in the last twenty-one years (2001–2021). *Veterinary Sciences, 9*(8), 384. https://doi.org/10.3390/vetsci9080384

Atanasov, A. G., Zotchev, S. B., Dirsch, V. M., & Supuran, C. T. (2021). Natural products in drug discovery: Progress and challenges. *Nature Reviews Drug Discovery*, *20*(3), 200–216. https://doi.org/10.1038/s41573-020-00114-z

Ayodele, O., & Sabiu, S. (2026). Integrated bioprospection of phenolics as potent modulators of *Acinetobacter baumannii* penicillin-binding protein 1A. *Journal of Chemistry*, *2026*, Article 6663249.

Baell, J. B., & Holloway, G. A. (2010). New substructure filters for removal of pan assay interference compounds (PAINS) from screening libraries and for their exclusion in bioassays. *Journal of Medicinal Chemistry*, *53*(7), 2719–2740. https://doi.org/10.1021/jm901137j

Bagheri Nejad, R., Krecek, R. C., Khalaf, O. H., Hailat, N., & Arenas-Gamboa, A. M. (2020). Brucellosis in the Middle East: Current situation and a pathway forward. *PLoS Neglected Tropical Diseases, 14*(5), e0008071. https://doi.org/10.1371/journal.pntd.0008071

Banerjee, P., Eckert, A. O., Schrey, A. K., & Preissner, R. (2018). ProTox-II: A webserver for the prediction of toxicity of chemicals. *Nucleic Acids Research, 46*(W1), W257–W263. https://doi.org/10.1093/nar/gky318

Daina, A., Michielin, O., & Zoete, V. (2017). SwissADME: A free web tool to evaluate pharmacokinetics, drug-likeness and medicinal chemistry friendliness of small molecules. *Scientific Reports, 7*, 42717. https://doi.org/10.1038/srep42717

D'Andrea, G. (2015). Quercetin: A flavonol with multifaceted therapeutic applications? *Fitoterapia, 106*, 256–271. https://doi.org/10.1016/j.fitote.2015.09.002

Dean, A. S., Crump, L., Greter, H., Hattendorf, J., Schelling, E., & Zinsstag, J. (2020). Clinical manifestations of human brucellosis: A systematic review and meta-analysis. *PLoS Neglected Tropical Diseases*, *14*(12), e0008570. https://doi.org/10.1371/journal.pntd.0008570

Donadio, G., Mensitieri, F., Santoro, V., Parisi, V., Bellone, M. L., De Tommasi, N., Izzo, V., & Dal Piaz, F. (2021). Interactions with microbial proteins driving the antibacterial activity of flavonoids. *Pharmaceutics, 13*(5), 660. https://doi.org/10.3390/pharmaceutics13050660

Ferri, M., Ranucci, E., Romagnoli, P., & Giaccone, V. (2017). Antimicrobial resistance: A global emerging threat to public health systems. *Critical Reviews in Food Science and Nutrition, 57*(13), 2857–2876. https://doi.org/10.1080/10408398.2015.1077192

Gaddafi, M. S., Jolayemi, K. O., Lawal, H., Musawa, I. A., Garba, B., Goni, M. D., & Amaje, J. (2026). Brucellosis prevalence in Nigerian livestock: A systematic review and meta-analysis. *BMC Infectious Diseases, 26,* Article 14210. https://doi.org/10.1186/s12879-026-14210-9

Guengerich, F. P. (2011). Mechanisms of drug toxicity and relevance to pharmaceutical development. *Drug Metabolism and Pharmacokinetics, 26*(1), 3–14. https://doi.org/10.2133/dmpk.DMPK-10-RV-062

Hamzah, K. J., Abady, N. R., Naji, M. Z., Saeed, S. I., Kamaruzzaman, N. F., & Goni, M. D. (2026). Genetic characterization and molecular docking of flavonoid compounds against *Klebsiella pneumoniae* and bovine herpesvirus type 1 (BoHV-1) isolated from clinical dairy cattle cases. *International Journal of Microbiology, 2026,* Article 8888183. https://doi.org/10.1155/ijm/8888183

Hull, N. C., & Schumaker, B. A. (2020). Comparisons of brucellosis between human and veterinary medicine. *Infectious Disease Reports, 12*(1), 8500. https://doi.org/10.4081/idr.2020.8500

Lavecchia, A. (2015). Machine-learning approaches in drug discovery: Methods and applications. *Drug Discovery Today, 20*(3), 318–331. https://doi.org/10.1016/j.drudis.2014.10.012

Lipinski, C. A., Lombardo, F., Dominy, B. W., & Feeney, P. J. (2001). Experimental and computational approaches to estimate solubility and permeability in drug discovery and development settings. *Advanced Drug Delivery Reviews, 46*(1–3), 3–26. https://doi.org/10.1016/S0169-409X(00)00129-0

Lopez-Novoa, J. M., Quiros, Y., Vicente, L., Morales, A. I., & Lopez-Hernandez, F. J. (2011). New insights into the mechanism of aminoglycoside nephrotoxicity: An integrative point of view. *Kidney International, 79*(1), 33–45. https://doi.org/10.1038/ki.2010.337

Maurice, N. A., Wungak, S. Y., Gana, B. A., Nanven, M. B., Ngbede, E. O., Ibrahim, A., Aworh, M. K., Konzing, L., Hambolu, S. E., & Gugong, V. T. (2013). Seroprevalence of bovine brucellosis in northern Plateau State, North Central Nigeria. *Asian Pacific Journal of Tropical Disease, 3*(5), 337–340. https://doi.org/10.1016/S2222-1808(13)60081-X

McDermott, J., Grace, D., & Zinsstag, J. (2021). Economics of the impact and control of brucellosis in livestock in low- and middle-income countries. *Frontiers in Veterinary Science*, *8*, 641460. https://doi.org/10.3389/fvets.2021.641460

Ojo, K. K., Ranade, R. M., Zhang, Z., Dranow, D. M., Myers, J. B., Choi, R., et al. (2016). *Brucella melitensis* methionyl-tRNA synthetase (MetRS), a potential drug target for brucellosis. *PLoS ONE, 11*(8), e0160350. https://doi.org/10.1371/journal.pone.0160350

Pappas, G., Akritidis, N., Bosilkovski, M., & Tsianos, E. (2005). Brucellosis. *New England Journal of Medicine*, *352*(22), 2325–2336. https://doi.org/10.1056/NEJMra050570

Pappas, G., Papadimitriou, P., Akritidis, N., Christou, L., & Tsianos, E. V. (2006). The new global map of human brucellosis. *The Lancet Infectious Diseases*, *6*(2), 91–99. https://doi.org/10.1016/S1473-3099(06)70382-6

Petersen, M., & Simmonds, M. S. J. (2003). Rosmarinic acid. *Phytochemistry*, *62*(2), 121–125. https://doi.org/10.1016/S0031-9422(02)00513-7

Rahman, M. T., Sobur, M. A., Islam, M. S., Ievy, S., Hossain, M. J., El Zowalaty, M. E., & Ashour, H. M. (2020). Zoonotic diseases: Etiology, impact, and control. *Microorganisms*, *8*(9), 1405. https://doi.org/10.3390/microorganisms8091405

Schrödinger LLC. (2023). *Schrödinger Release 2023-2: Maestro*. Schrödinger LLC.

Sharifi-Rad, J., Sureda, A., Tenore, G. C., Daglia, M., Sharifi-Rad, M., Valussi, M., Tundis, R., Sharifi-Rad, M., Loizzo, M. R., Ademiluyi, A. O., Sharifi-Rad, R., Ayatollahi, S. A., & Iriti, M. (2017). Biological activities of essential oils: From plant chemoecology to traditional healing systems. *Molecules*, *22*(1), 70. https://doi.org/10.3390/molecules22010070

Sharifi-Rad, M., Yılmaz, Y. B., Antika, G., Salehi, B., Tumer, T. B., Kulandaisamy Venil, C., Das, G., Patra, J. K., Karazhan, N., Akram, M., Iqbal, M., Imran, M., Sen, S., Acharya, K., Dey, A., & Sharifi-Rad, J. (2021). Phytochemical constituents, biological activities, and health-promoting effects of the genus *Origanum*. *Phytotherapy Research*, *35*(1), 95–121. https://doi.org/10.1002/ptr.6785

Sliwoski, G., Kothiwale, S., Meiler, J., & Lowe, E. W. (2014). Computational methods in drug discovery. *Pharmacological Reviews, 66*(1), 334–395. https://doi.org/10.1124/pr.112.007336

World Health Organization. (2022a). *Brucellosis*. World Health Organization.

World Health Organization. (2022b). *Global health estimates: Life expectancy and leading causes of death and disability*. World Health Organization.

World Health Organization. (2023). *WHO model list of essential medicines* (23rd ed.). World Health Organization.

Zhao, T., Zhang, Y., Liu, L., et al. (2023). Systems pharmacology reveals the potential targets and signalling mechanisms in the adjuvant treatment of brucellosis with traditional Chinese medicine. *ACS Omega, 8*(31), 28797–28812. https://doi.org/10.1021/acsomega.3c03603

Zheng, R., Xie, S., Lu, X., Sun, L., Zhou, Y., Zhang, Y., & Wang, K. (2018). A systematic review and meta-analysis of epidemiology and clinical manifestations of human brucellosis in China. *BioMed Research International, 2018*, Article 5712920. https://doi.org/10.1155/2018/5712920